



Anomalous non-Hermitian skin effect: topological inequivalence of skin modes versus point gap

Gang-Feng Guo¹, Xi-Xi Bao², Han-Jie Zhu³, Xiao-Ming Zhao⁴, Lin Zhuang⁵, Lei Tan^{1,6} & Wu-Ming Liu³

It has long been believed that skin modes are equivalent to the nontrivial point gap. However, we find that this concomitance can be broken, in that skin modes can be absent or present when the point gap is nontrivial or trivial, respectively, named anomalous non-Hermitian skin effect. This anomalous phenomenon arises whenever unidirectional hopping amplitudes emerge among subsystems, where sub-chains have decoupling-like behaviors and contribute only to the energy levels without particle occupation. The occurrence of anomalous non-Hermitian skin effect is accompanied by changes in open boundary eigenvalues, whose structure exhibits multifold exceptional points and can not be recovered by continuum bands. Moreover, an experimental setup is proposed to simulate this effect. Our results reveal the topologically inequivalence of skin modes and point gap. This effect not only provides a deeper understanding of non-Bloch theory and critical phenomena, but may inspire applications, such as in sensor field.

¹Lanzhou Center for Theoretical Physics, Key Laboratory of Theoretical Physics of Gansu Province, Lanzhou University, Lanzhou, China. ²College of Mathematics and Physics, Suqian University, Suqian, China. ³Beijing National Laboratory for Condensed Matter Physics, Institute of Physics, Chinese Academy of Sciences, Beijing, China. ⁴Department of Physics and Institute of Theoretical Physics, University of Science and Technology Beijing, Beijing, China. ⁵State Key Laboratory of Optoelectronic Materials and Technologies, School of Physics, Sun Yat-Sen University, Guangzhou, China. ⁶Key Laboratory for Magnetism and Magnetic Materials of the Ministry of Education, Lanzhou University, Lanzhou, China. ✉email: stszhl@mail.sysu.edu.cn; tanlei@lzu.edu.cn; wliu@iphy.ac.cn

Recent theoretical and experimental studies on non-Hermitian systems have revealed many interesting phenomena without Hermitian counterparts, and thus greatly expanded our cognition of physics laws^{1–18}. A quintessential feature of non-Hermitian systems is skin modes^{19–26}, which are the accumulation of the majority of eigenstates at system boundaries. The non-Hermitian skin effect causes nullities of conventional bulk-boundary correspondence¹⁹. Specifically, the eigenvalues under different boundary conditions have a crucial distinction. Non-Bloch band theory was subsequently proposed, from which generalized Brillouin zone and continuum bands can be obtained to redefine the topological invariant and reproduce the open boundary band structures^{19,20}. The exotic accumulation phenomenon of the eigenstates has important applications for topological sensors^{27,28}, the integrated optical chip²⁹, and topological lasing^{30,31}. Presently, it is widely believed that the non-Hermitian skin effect is tantamount to the topologically nontrivial point gap^{21,32–37} and vice versa, which can be explained as follows. The Hamiltonian under open boundary conditions is always topologically trivial for the point gap. Thus, if the Hamiltonian under periodic boundary conditions is nontrivial, the non-Hermitian skin effect is present inevitably [Fig. 1].

However, we reveal that open boundary eigenstates can exhibit anomalous non-Hermitian skin effect, where skin modes can be ever absent even though the point gap is nontrivial, whereas skin modes are present for trivial point gap. This phenomenon occurs only when unidirectional hopping leading to decoupling-like behaviors is considered, where some subsystems contribute only to energy levels under periodic boundaries, and have no eigenstate distribution under open boundary conditions. That is to say, the curve in momentum space formed by the Bloch Hamiltonian will have a loop around a reference point and all sub-chains of the system affect the point gap. Yet under open boundary conditions, there is no wave function distribution on some sub-chains. With the emergence of the inequivalence of skin modes and point gap,

there is a sudden change in open boundary eigenvalues. Specifically, there are multifold exceptional points, whose degree of degeneracy is proportional to the system size, among the open boundary eigenvalues that are appreciably different from the continuum bands. The physical properties of the eigenvalues may have relevance in the field of sensors. Finally, an experimental setup with electric circuits is proposed to realize our system.

Results

We consider a non-Hermitian three-band system (Fig. 2a), whose Hamiltonian reads as

$$H = \sum_{n=1}^N \left[t_a C_{A,n+1}^\dagger C_{A,n} + t_c C_{C,n}^\dagger C_{C,n+1} + t_b (C_{B,n}^\dagger C_{B,n+1} + C_{B,n+1}^\dagger C_{B,n}) + \gamma_1 C_{A,n}^\dagger C_{B,n} + \gamma_2 C_{B,n}^\dagger C_{A,n} + \gamma_3 C_{B,n}^\dagger C_{C,n} + \gamma_4 C_{C,n}^\dagger C_{B,n} + V_a C_{A,n}^\dagger C_{A,n} + V_b C_{B,n}^\dagger C_{B,n} + V_c C_{C,n}^\dagger C_{C,n} \right], \quad (1)$$

where $C_{A,n}^\dagger$ ($C_{A,n}$), $C_{B,n}^\dagger$ ($C_{B,n}$) and $C_{C,n}^\dagger$ ($C_{C,n}$) represent the creation (annihilation) operators for sublattice A, B and C in the n -th unit cell. For sub-chain A, only right hopping t_a is considered. Conversely, only left tunneling t_c is considered for sub-chain C. Meanwhile, sub-chain B is Hermitian with the hopping amplitude being t_b . γ_1 and γ_2 stand for non-Hermitian hopping between A and B sub-chain, while γ_3 and γ_4 are non-Hermitian hopping between B and C sub-chain. V_a , V_b and V_c stand for the on-site potentials for sub-chains A, B and C, respectively. Without loss of generality, we take all parameters as real numbers.

We start with normal case for comparison. The non-Hermitian skin effect can be generally confirmed by nontrivial point gap, or equivalently, by non-zero spectral winding $W = \frac{1}{2\pi i} \int_0^{2\pi} dk \partial_k \ln \det[H(k) - E_b]$ ^{21,33–36}, where E_b is an arbitrary reference point. As an example, we can choose $E_b = \frac{1}{2}i$ and $W = 1$ will be received [see Supplementary Note II for more

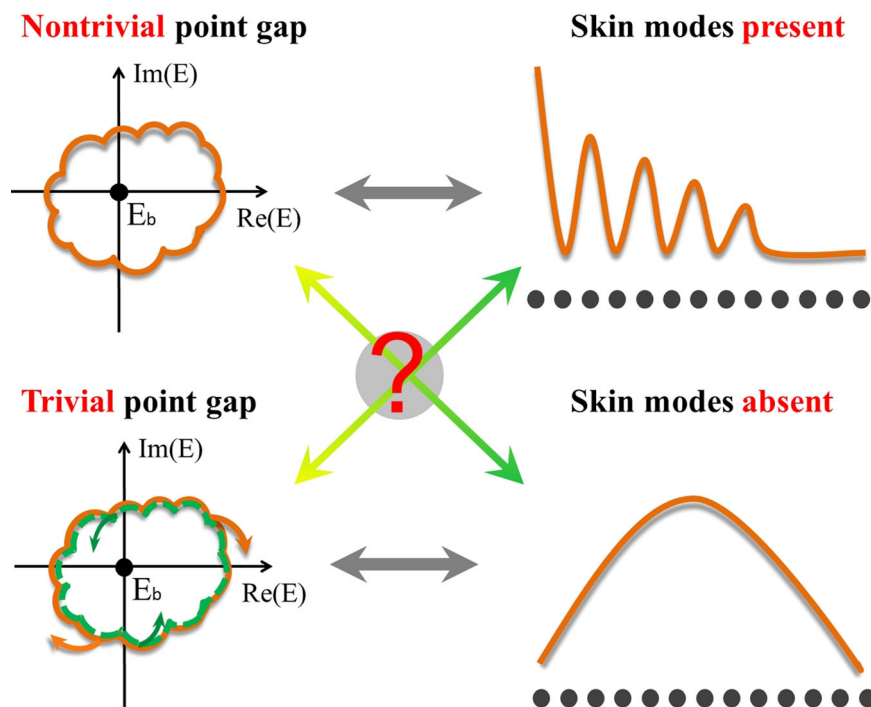


Fig. 1 Relationship between point gap and the non-Hermitian skin effect. It is taken for granted that the topologically nontrivial (trivial) point gap is equivalent to the presence (absence) of skin modes. However, we question whether this is a universal conclusion. In our work, we exhibit a consequence of the anomalous non-Hermitian skin effect: the open boundary eigenstates being localized for the topologically trivial point gap while extended for the nontrivial point gap.

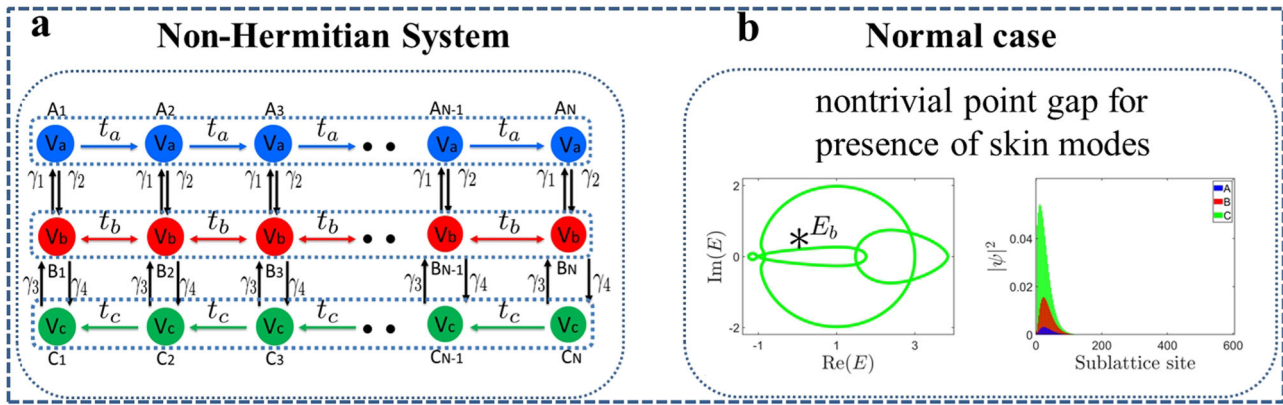


Fig. 2 Brief of the non-Bloch band theory. **a** Non-Hermitian three-band system with the number of unit cells N . t_a (V_a), t_b (V_b) and t_c (V_c) are the hopping amplitudes (on-site potentials) for sub-chain A, B and C, respectively. γ_i ($i = 1, 2, 3, 4$) stands for couplings between sub-chains. **b** Normal case that the topologically nontrivial point gap stands for the occurrence of skin modes. The green curve encircling the reference point $E_b = \frac{1}{2}i$ in left sub-figure is eigenvalues under periodic boundary conditions, and therefore non-Hermitian skin effect is displayed in the right sub-figure. The parameters are $N = 200$, $t_a = 1$, $t_b = \frac{4}{5}$, $t_c = 2$, $\gamma_1 = \gamma_2 = 1$, $\gamma_3 = \frac{1}{10}$, $\gamma_4 = \frac{1}{2}$, $V_a = 2$ and $V_b = V_c = 1$.

details]. The system thus holds non-Hermitian skin modes, as shown in Fig. 2b. Specifically, all sub-chains have distributions of open boundary eigenstates.

Anomalous absence of skin modes for nontrivial point gap. We now explore the localization properties of open boundary eigenstates under unidirectional hopping amplitudes ($\gamma_1 = \gamma_4 = 0$). In this case, three eigenvalue branches in momentum space are $E_{k1} = V_a + t_a e^{-ik}$, $E_{k2} = V_c + t_c e^{ik}$ and $E_{k3} = V_b + 2t_b \cos(k)$. The complex energy spectra E_{k1} (E_{k2}) will rotate clockwise (counterclockwise) on the complex plane, and E_{k3} simply forms a line as k varies from 0 to 2π . Therefore, as long as $V_a \neq V_c$ or $t_a \neq t_c$, there must exist a reference point E_b (Here we can choose $E_b = \frac{1}{2}i$) surrounded only once and the area of the curve must be nonzero³⁶, as shown in Fig. 3a. Hence, it seems that our system exhibits the non-Hermitian skin effect.

However, in addition to adopting an indirect perspective of the point gap in momentum space, i.e., from the Bloch Hamiltonian to analyze the skin modes, we can directly examine the distributions of eigenstates under open boundary conditions and find that the conclusion mentioned above is not suitable. To characterize the localization properties of all wave functions quantitatively, the inverse participation ratio (IPR) is introduced as $IPR^s = \frac{(\sum_{i=1}^N |\Psi_i^s|^4)}{(\sum_{i=1}^N |\Psi_i^s|^2)^2}$ for the s -th eigenstate $|\Psi^s\rangle$ ^{38,39}.

For large system size, IPR^s is finite for the localized eigenstate, whereas it approaches zero for extended eigenstate. As shown in Fig. 3b, $IPR^s \equiv 0.0075$, which indicates that all eigenstates should be extended, not localized on open chain. One eigenvalue in Fig. 3b can be selected to exhibit the distribution of the eigenstates. As shown in Fig. 3c, the open boundary eigenstates are indeed extended only on the B sub-chain, which conforms to the non-Hermitian skin effect disappearance numerically. We further plot the distribution of all open boundary eigenstates corresponding to eigenvalues in Fig. 3d. There is no large number of eigenstates localized at system boundary, i.e., the non-Hermitian skin effect is absent whereas the point gap is nontrivial. Physically, sub-chain A (C) has only unidirectional hopping to sub-chain B, but the reverse does not happen when $\gamma_1 = 0$ ($\gamma_4 = 0$), and B sub-chain is Hermitian, which can be solved analytically (Supplementary Note II). Hence, there is no probability distribution on sub-chain A (C), and Bloch waves survive in B sub-chain (Fig. 3e).

Anomalous presence of skin mode for trivial point gap. The non-Hermitian skin effect is present at unidirectional hopping amplitudes for $\gamma_1 = \gamma_3 = 0$. To confirm that the spectral winding number is zero, corresponding to trivial point gap, conditions of the Hamiltonian (1) are further restricted as $V_a = V_c$ and $t_a = t_c$, i.e., generalized Brillouin zone of non-Hermitian three-band Hamiltonian (1) is a unit circle (Supplementary Note I). In addition to quantitative calculations of spectral windings, topological properties of the point gap can be gained intuitively. Namely, if the area of the curve surrounded by $(\text{Re}[\det[H(k)]], \text{Im}[\det[H(k)]])$ is zero, non-Hermitian skin modes will vanish and vice versa^{21,33–36}. For our system, three eigenvalue branches in momentum space satisfy $|E_{k1}| = |V_a + t_a e^{-ik}| = |E_{k2}| = |V_c + t_c e^{ik}|$ and $E_{k3} = V_b + 2t_b \cos(k)$, i.e., E_{k1} and E_{k2} will trace two circles with same radius but in opposite direction of rotation when k changes from 0 to 2π [Fig. 3f]. Therefore, for any reference point E_b , the spectral winding is equal to zero exactly, and it seems that there is no non-Hermitian skin effect.

However, we can also examine the localization properties of open boundary eigenstates from IPR^s. As shown in Fig. 3g, $\min(IPR^s) = 0.9406$ as the energy changes under numerical simulation, which means that all eigenstates are localized, rather than extended, even if spectral winding number is constantly zero. Here, the information on the exceptional points [discussed next] and the corresponding eigenstates has been excluded. We can arbitrarily present the distribution of an open boundary eigenstate in Fig. 3h. It is obviously localized at the left C sub-chain of the system. Furthermore, Fig. 3i presents the distribution of all open boundary eigenstates associated with eigenvalues, where eigenstates have been normalized. Globally, all open boundary eigenstates are pinned at the left system boundaries, i.e., the non-Hermitian skin effect is present. Physically, one can analytically find that there only exists unidirectional hopping from sub-chain A to a subsystem comprising sub-chains B and C when $\gamma_1 = 0$ [Supplementary Note II], and this subsystem is still non-Hermitian essentially. Hence, there is no probability distribution on sub-chain A, while the non-Hermitian skin effect also can be exhibited in the subsystem (Fig. 3j).

Changes of open boundary eigenvalues. We now analyze the properties of energy spectrum when anomalous non-Hermitian skin effect occurs. According to Hamiltonian (1), the characteristic polynomial of our system is

$$f(\beta, E) = a_2\beta^2 + a_1\beta^1 + a_0\beta^0 + a_{-1}\beta^{-1} + a_{-2}\beta^{-2} = 0. \quad (2)$$

Anomalous case

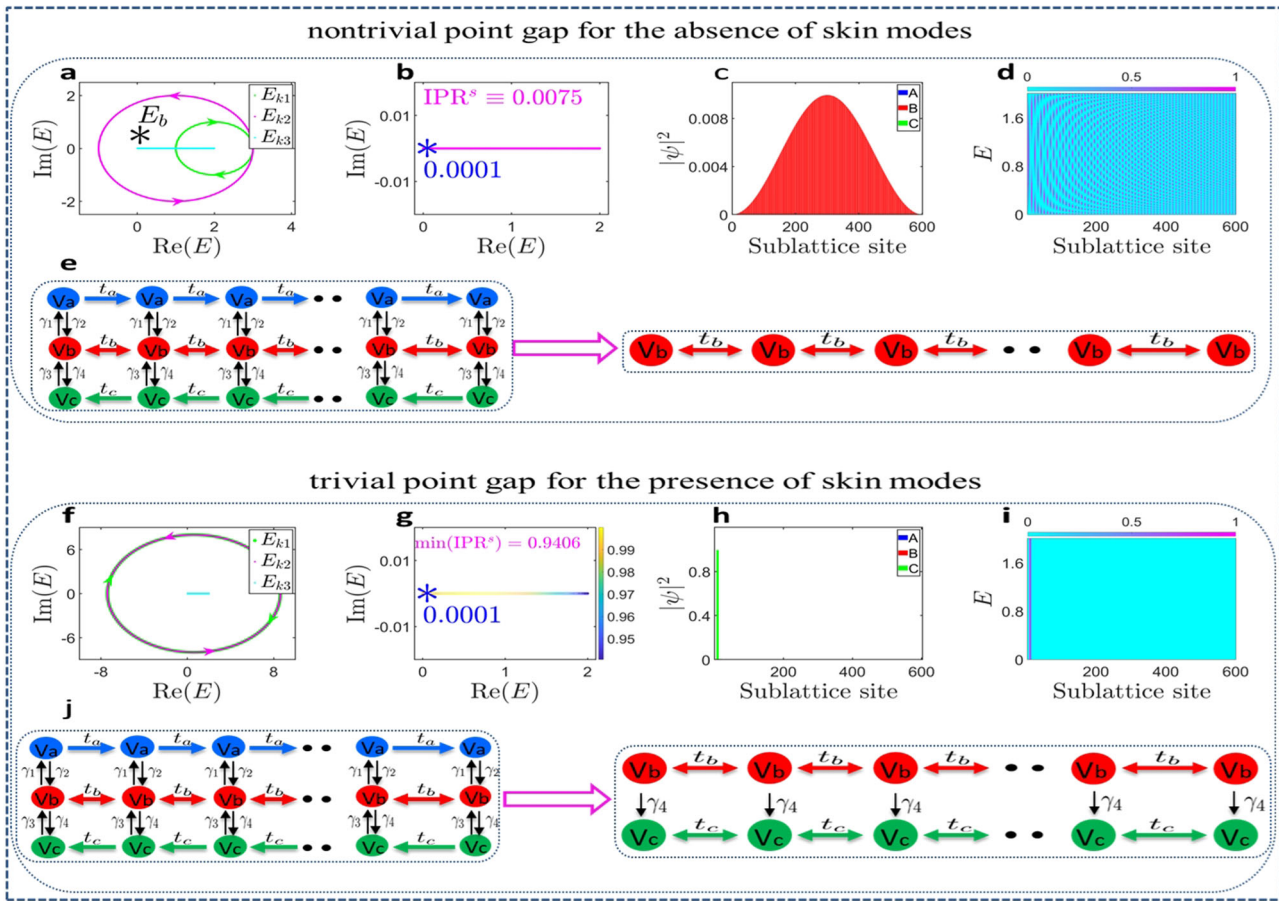


Fig. 3 Anomalous non-Hermitian skin effect. **a** Nontrivial point gap obtained from $(\text{Re}[\det[H(k)]], \text{Im}[\det[H(k)]])$ as k varies from 0 to 2π for the reference point $E_b = \frac{1}{2}i$. Namely, the effects of all energy bands are taken into account in calculation of spectral winding. **b** Open boundary eigenvalues colored by their inverse participation ratio for the s -th eigenstate $|\Psi^s\rangle$ (IPR^s), remaining constant approaching zero. **c** Distribution of the open boundary eigenstate corresponding to the blue asterisk $E_{OBC} = 0.0001$ in **b**, where occupation is non-zero only on sub-chain B, while both sub-chain A and sub-chain C have no occupation. **d** Normalized eigenstates with the change of eigenvalues. All eigenstates are extended, rather than localized, on the open chain. **e** Non-Hermitian three-band system will be simplified as a Hermitian one-band model when $\gamma_1 = \gamma_4 = 0$. **f** Momentum space spectra, where E_{k1} and E_{k2} will display two circles with the same radius but opposite rotation directions when k changes from 0 to 2π . Thus, the point gap is topologically trivial for any reference point. In other words, all energy levels in momentum space contribute to the point gap. **g** Open boundary eigenvalues. Different colors are different values of IPR^s , which is finite for the corresponding eigenstate. **h** Distribution of the open boundary eigenstate, which is localized, rather than extended. **i** Eigenstates as a function of all open boundary eigenvalues E . All eigenstates have been normalized and are localized at the boundaries of the system. The A sub-chain only contributes the energy level while without wavefunction distribution. **j** Open boundary non-Hermitian three-band system will become the non-Hermitian two-band system from both eigenstates and eigenvalues perspectives when $\gamma_1 = \gamma_3 = 0$. The parameters for **a-e** are $\gamma_1 = \gamma_4 = 0$, $t_a = 1$, $t_b = \frac{1}{2}$, $t_c = 2$, $\gamma_2 = 2$, $\gamma_3 = 1$, $V_a = 2$ and $V_b = V_c = 1$. **f-j** $\gamma_1 = \gamma_3 = 0$, $t_a = t_c = 8$, $t_b = \frac{1}{2}$, $\gamma_2 = 2$, $\gamma_4 = 1$, $V_a = V_c = \frac{3}{5}$ and $V_b = 1$.

The coefficients from a_2 to a_{-2} can be seen in Supplementary Note I. The characteristic polynomial $f(\beta, E)$ is a quartic equation. The solutions can be numbered as $|\beta_1| \leq |\beta_2| \leq |\beta_3| \leq |\beta_4|$ for a given E and $|\beta_2| = |\beta_3|$ is required to determine generalized Brillouin zone and derivative continuum bands. As shown in Fig. 4a, generalized Brillouin zone is displayed, and correspondingly, the open boundary energy spectrum is well recovered by continuum bands with $\gamma_1 = \frac{1}{500}$ and $\gamma_4 = \frac{1}{400}$ (Fig. 4b).

However, the situation is remarkably different when $\gamma_1 = \gamma_4 = 0$, corresponding to presence anomalous non-Hermitian skin effect. Generalized Brillouin zone shown in Fig. 4c is slightly different from the one in Fig. 4a, and there is very little change for continuum bands [comparing red curve in Fig. 4b with the one in Fig. 4d], while open boundary eigenvalues differ and lie on the real axis. Hence, open boundary energies and continuum bands will not be compatible with each other.

Further, it is taken for granted that if every open boundary eigenvalue is brought into the characteristic polynomial $f(\beta, E)$, and the second and third largest $|\beta|$ are selected, the data should belong to generalized Brillouin zone obtained from non-Bloch band theory^{19–21,26,40}. However, unlike the case in the established scenarios, this rule is nullified in singular phenomenon. Detailedly, we can choose an open eigenvalue in Fig. 4d, such as $E_{OBC} = 4$, and bring it into the characteristic polynomial $f(\beta, E)$. After calculation, one can receive $\{|\beta_1|, |\beta_2|, |\beta_3|, |\beta_4|\}_{E=4} = \{0.6667, 1.000, 1.000, 4.000\}$, i.e., $|\beta_2| = |\beta_3|$. This equality is exactly the condition of obtaining generalized Brillouin zone and corresponding continuum bands. Therefore, $E_{OBC} = 4$ can be reproduced by continuum bands based on non-Bloch band theory⁴⁰. Yet, another open boundary eigenvalue $E_{OBC} = \frac{6}{5}$ can be considered as well. Similarly, $\{|\beta_1|, |\beta_2|, |\beta_3|, |\beta_4|\}_{E=\frac{6}{5}} = \{1.000, 1.000, 1.600, 10.00\}$, i.e., $|\beta_2| \neq |\beta_3|$ but $|\beta_1| = |\beta_2|$.

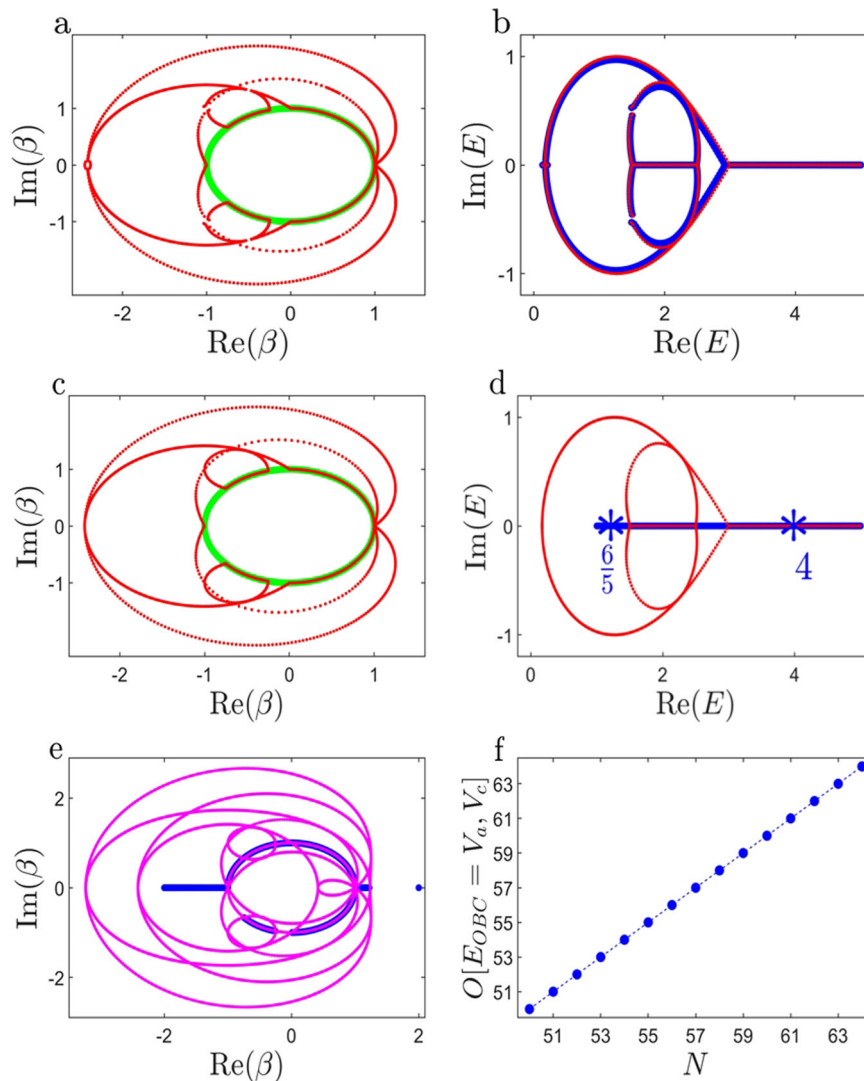


Fig. 4 Changes in open boundary eigenvalues. **a** Generalized Brillouin zone (red curve) and Brillouin zone (green curve). **b** Energy spectra under open boundary conditions (blue curve) and continuum bands (red curve). **c** Generalized Brillouin zone (red curve) and Brillouin zone (green curve). **d** Energy spectra under open boundary conditions (blue curve) and continuum bands (red curve). After bringing two open boundary eigenvalues into $f(\beta, E)$, one energy value obtains $|\beta_2| = |\beta_3|$ ($E_{OBC} = 4$) while the other corresponds to $|\beta_1| = |\beta_2|$ ($E_{OBC} = \frac{6}{5}$). **e** Auxiliary generalized Brillouin zone (red curve) containing all information of $|\beta_m| = |\beta_n|$ ($\{m, n\} = \{1, 2, 3, 4\}$) with $f(\beta, E) = 0$, and generalized Brillouin zone obtained from the open boundary eigenvalues (blue curve). **f** Number of certain open boundary eigenvalues versus the system size. **a** and **b** $\gamma_1 = \frac{1}{500}$ and $\gamma_4 = \frac{1}{400}$. **c-f** $\gamma_1 = \gamma_4 = 0$. Other parameters: $t_a = 2$, $t_b = 1$, $t_c = \frac{1}{2}$, $\gamma_2 = 1$, $\gamma_3 = \frac{1}{10}$, $V_a = 1V_b = 3$ and $V_c = 2$.

Evidently, this equality contradicts the condition of obtaining generalized Brillouin zone, i.e., this open boundary eigenvalue must not belong to continuum bands determined by $|\beta_2| = |\beta_3|$. Figure 4d visually confirms these results.

The singular energy spectrum can also be examined from a more general perspective. In Ref. 26, authors proposed a concept of the auxiliary generalized Brillouin zone, which is obtained by solving the characteristic equation $f(\beta, E) = 0$ when E takes every value of the complex number field with $|\beta_m| = |\beta_n|$ ($\{m, n\} = \{1, 2, 3, 4\}$). However, as shown in Fig. 4e, even though the auxiliary generalized Brillouin zone possesses all equality information of $f(\beta, E) = 0$, it remains impossible to recover generalized Brillouin zone obtained from open boundary eigenvalues. This further confirms the emergence of singular energy spectrum.

Meanwhile, we analytically exhibit that the determinant of open boundary Hamiltonian has the form $\det[H_{OBC} - E_{OBC}; N \times N] = 2^{-N}(V_a - E_{OBC})^N(V_c - E_{OBC})^N\gamma(V_b, t_b, E_{OBC})$ with unidirectional

hopping being satisfied (Supplementary Note II), with N being total number of the system size. Hence, $E_{OBC} = V_a$ and $E_{OBC} = V_c$ must be solutions of $\det[H_{OBC} - E_{OBC}; N \times N] = 0$, and be N -fold exceptional points^{41,42}. In Fig. 4f, we exhibit the number of the open boundary eigenvalues of $E_{OBC} = V_a$ and $E_{OBC} = V_c$ with different system sizes. Explicitly, the number of degeneracy points is proportional to the system size.

Additionally, sensors have penetrated aspects of daily life. The core part of a sensor is transformation circuit, which amplifies weak signals⁴³⁻⁴⁵. Interestingly, it has been displayed that minute perturbations of parameters will affect the eigenvalues. Moreover, Refs. 46-51 also show that higher-order exceptional points have advantages for sensor applications, and it is significant to seek higher-order exceptional points in various systems. Coincidentally, we also have shown that the emergence of the singular phenomenon is accompanied by the multifold exceptional point. Hence, our non-Hermitian systems may have potential applications in the sensor field.

Proposed experimental implementation. There exist several physical incarnations that can be used to explore non-Hermitian systems^{52–68}, including cold atoms^{52–55}, electrical circuits^{56–63}, photonic and acoustic systems^{64–68}. Among them, electric circuits have been widely used because the circuit structure can be flexibly designed to facilitate integration and mass production. Here, we propose an experimental scheme to realize our system through electric circuits (Supplementary Note III). The essential part of the electric system is the negative converter with current inversion (INIC), the impedance of which is changed from negative to positive with the orientation of the current being reversed, or vice versa, as shown in Fig. 5. Our system can be achieved by choosing appropriate impedances for these electric devices. Explicitly, the parameters of the devices are $Y_{A1} = V_a$, $Y_{Aj} = V_a + t_a (1 < j \leq N)$, $Y'_{Aj} = -\gamma_1$, $Y_{AB} = -\frac{\gamma_1 + \gamma_2}{2}$, $Y'_{AB} = \frac{\gamma_1 - \gamma_2}{2}$, $Y_{AA} = Y'_{AA} = -\frac{t_a}{2}$, $Y_{B1} = Y_{BN} = V_b$, $Y_{Bj} = V_b + t_b (1 < j < N)$, $Y_{BC} = -\frac{\gamma_3 + \gamma_4}{2}$, $Y'_{BC} = \frac{\gamma_3 - \gamma_4}{2}$, $Y_{BB} = -t_b$, $Y_{Cj} = V_c (1 \leq j < N)$, $Y_{CN} = V_c - t_c$, $Y'_{Cj} = -(\gamma_4 + t_c)$, $Y_{CC} = -\frac{t_c}{2}$ and $Y'_{CC} = \frac{t_c}{2}$.

Conclusion

We unravel that open boundary eigenstates exhibit an anomalous non-Hermitian skin effect in which they are extended for the topologically nontrivial point gap but localized for trivial point gap, provided that there are one-directional coupling amplitudes among the sub-chains. Additionally, with the presence of

anomalous non-Hermitian skin effect, open boundary eigenvalues will have wide distinction compared with continuum bands. Notably, there exist multifold exceptional points in an open chain, and the degree of degeneracy grows as the system size increases. The physical properties of the eigenvalues may have applications in sensors field. Our results presented here demonstrate the unique irrelevance of the non-Hermitian skin effect and point gap, which could advance non-Bloch theory and our understanding of critical phenomenon in non-Hermitian field. Meanwhile, the conclusions can be generalized to various non-Hermitian systems (such as the four-band system in Supplementary Note IV).

Methods

The spectral winding number defined as $W = \frac{1}{2\pi i} \int_0^{2\pi} dk \partial_k \ln \det[H(k) - E_b]$ ^{21,33–36} can be calculated quantitatively from the residue theorem via $e^{ik} \rightarrow z$ and $dk \rightarrow \frac{1}{iz} dz$.

Such as, one can see that five first-order poles are distributed on the complex plane for a given $E_{b1} = \frac{1}{6}i$ in Fig. 6a, where four of them are contributed to spectral winding and $W = 1$ can be obtained, i.e., the point gap is topologically nontrivial. However, three poles are surrounded by the unit circle in Fig. 6b for different parameters and the point gap is trivial. Precisely, the spectral winding $W \equiv 0$ for any reference point as long as $t_a = t_c$, $V_a = V_c$ and $\gamma_1\gamma_2 = \gamma_3\gamma_4$ (Supplementary Note II).

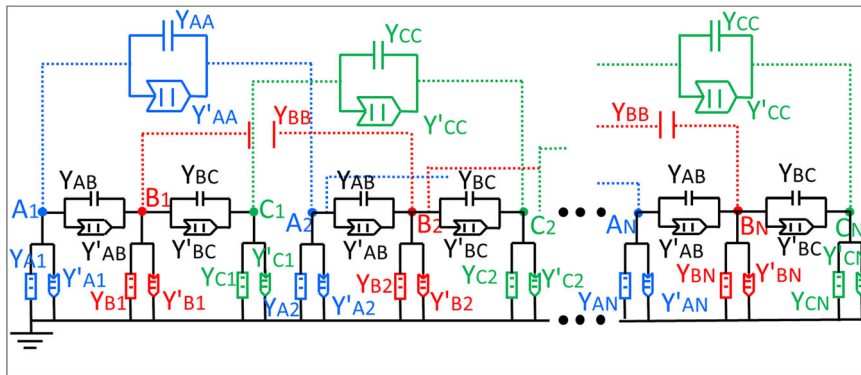


Fig. 5 Proposed electric circuit configurations for realizing the Hamiltonian. The Hamiltonian is given in Eq. (1). The electric elements contain the negative converter with current inversion (INIC), capacitor and wires. Y_{AA} , Y_{BB} and Y_{CC} are capacitance of the capacitor. Y'_{AA} and Y'_{CC} are capacitance of the INIC for a capacitor. A sub-chain, B sub-chain and C sub-chain are respectively connected by those electric devices. Y_{AB} and Y'_{AB} being respectively the capacitance of the capacitor and INIC for a capacitor connect A sub-chain and B sub-chain, while Y_{BC} and Y'_{BC} connect B sub-chain and C sub-chain. On-site potential is obtained by grounding each node with suitable circuit devices.

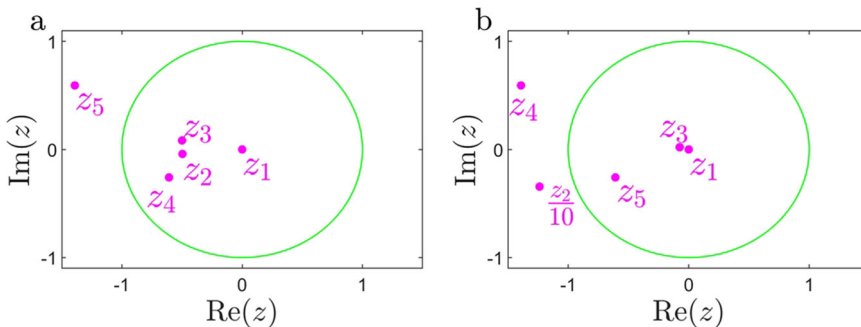


Fig. 6 Distribution of poles under anomalous non-Hermitian skin effect. **a** z_1, z_2, z_3 and z_4 being encircled by the unit circle, which induces the nonzero spectral winding, or the nontrivial point gap. Parameters are $E_{b1} = \frac{1}{6}i$, $\gamma_1 = \gamma_4 = 0$, $t_a = 1$, $t_b = \frac{1}{2}$, $t_c = 2$, $\gamma_2 = 2$, $\gamma_3 = 1$, $V_a = 2$ and $V_b = V_c = 1$. **b** z_1, z_3 and z_5 being encircled by the unit circle, while z_2 and z_4 being excluded for reference point $E_{b2} = \frac{1}{6}i$. Thus, the system corresponds to the trivial point gap. Parameters are $\gamma_1 = \gamma_3 = 0$, $t_a = t_c = 8$, $t_b = \frac{1}{2}$, $\gamma_2 = 2$, $\gamma_4 = 1$, $V_a = V_c = \frac{3}{5}$ and $V_b = 1$.

Data availability

The data in this manuscript are available from the authors upon reasonable request.

Code availability

The code used for the analysis is available from the authors upon reasonable request.

Received: 10 May 2023; Accepted: 29 November 2023;

Published online: 19 December 2023

References

1. Franca, S., Könye, V., Hassler, F., van den Brink, J. & Fulga, C. Non-Hermitian physics without gain or loss: the skin effect of reflected waves. *Phys. Rev. Lett.* **129**, 086601 (2022).
2. Xue, W.-T., Hu, Y.-M., Song, F. & Wang, Z. Non-Hermitian edge burst. *Phys. Rev. Lett.* **128**, 120401 (2022).
3. Abbasi, M., Chen, W., Naghiloo, M., Joglekar, Y. N. & Murch, K. W. Topological quantum state control through exceptional-point proximity. *Phys. Rev. Lett.* **128**, 160401 (2022).
4. Li, Y., Liang, C., Wang, C., Lu, C. & Liu, Y.-C. Gain-loss-induced hybrid skin-topological effect. *Phys. Rev. Lett.* **128**, 223903 (2022).
5. Wang, Q., Zhu, C., Wang, Y., Zhang, B. & Chong, Y. D. Amplification of quantum signals by the non-Hermitian skin effect. *Phys. Rev. B* **106**, 024301 (2022).
6. Song, F., Yao, S. & Wang, Z. Non-Hermitian skin effect and chiral damping in open quantum systems. *Phys. Rev. Lett.* **123**, 170401 (2019).
7. Vecsei, P. M., Denner, M. M., Neupert, T. & Schindler, F. Symmetry indicators for inversion-symmetric non-Hermitian topological band structures. *Phys. Rev. B* **103**, L201114 (2021).
8. Okugawa, R., Takahashi, R. & Yokomizo, K. Non-Hermitian band topology with generalized inversion symmetry. *Phys. Rev. B* **103**, 205205 (2021).
9. Yoshida, T., Okugawa, R. & Hatsugai, Y. Discriminant indicators with generalized inversion symmetry. *Phys. Rev. B* **105**, 085109 (2022).
10. Guo, C.-X., Liu, C.-H., Zhao, X.-M., Liu, Y. & Chen, S. Exact solution of non-hermitian systems with generalized boundary conditions: size-dependent boundary effect and fragility of the skin effect. *Phys. Rev. Lett.* **127**, 116801 (2021).
11. Kawabata, K., Okuma, N. & Sato, M. Non-Bloch band theory of non-Hermitian Hamiltonians in the symplectic class. *Phys. Rev. B* **101**, 195147 (2020).
12. Zhu, W., Teo, W. X., Li, L. & Gong, J. Delocalization of topological edge states. *Phys. Rev. B* **103**, 195414 (2021).
13. Li, L., Lee, C. H., Mu, S. & Gong, J. Critical non-Hermitian skin effect. *Nat. Commun.* **11**, 5491 (2020).
14. Liu, T. et al. Second-order topological phases in non-hermitian systems. *Phys. Rev. Lett.* **122**, 076801 (2019).
15. Leykam, D., Bliokh, K. Y., Huang, C., Chong, Y. D. & Nori, F. Edge modes, degeneracies, and topological numbers in non-hermitian systems. *Phys. Rev. Lett.* **118**, 040401 (2017).
16. Liu, T., He, J. J., Yang, Z. & Nori, F. Higher-order weyl-exceptional-ring semimetals. *Phys. Rev. Lett.* **127**, 196801 (2021).
17. Bliokh, K. Y., Leykam, D., Lein, M. & Nori, F. Topological non-Hermitian origin of surface Maxwell waves. *Nat. Commun.* **10**, 580 (2019).
18. Ge, Z.-Y. et al. Topological band theory for non-Hermitian systems from the Dirac equation. *Phys. Rev. B* **100**, 054105 (2019).
19. Yao, S. & Wang, Z. Edge states and topological invariants of non-hermitian systems. *Phys. Rev. Lett.* **121**, 086803 (2018).
20. Yokomizo, K. & Murakami, S. Non-bloch band theory of non-hermitian systems. *Phys. Rev. Lett.* **123**, 066404 (2019).
21. Zhang, K., Yang, Z. & Fang, C. Correspondence between winding numbers and skin modes in non-Hermitian systems. *Phys. Rev. Lett.* **125**, 126402 (2020).
22. Zhu, P., Sun, X.-Q., Hughes, T. L. & Bahl, G. Higher rank chirality and non-Hermitian skin effect in a topoelectrical circuit. *Nat. Commun.* **14**, 720 (2023).
23. Gu, Z. et al. Transient non-Hermitian skin effect. *Nat. Commun.* **13**, 7668 (2022).
24. Lee, T. E. Anomalous edge state in a non-hermitian lattice. *Phys. Rev. Lett.* **116**, 133903 (2016).
25. Zhang, X., Tian, Y., Jiang, J.-H., Lu, M.-H. & Chen, Y.-F. Observation of higher-order non-Hermitian skin effect. *Nat. Commun.* **12**, 5377 (2021).
26. Yang, Z., Zhang, K., Fang, C. & Hu, J. Non-hermitian bulk-boundary correspondence and auxiliary generalized Brillouin zone theory. *Phys. Rev. Lett.* **125**, 226402 (2020).
27. Budich, J. C. & Bergholtz, E. J. Non-hermitian topological sensors. *Phys. Rev. Lett.* **125**, 180403 (2020).
28. McDonald, A. & Clerk, A. A. Exponentially-enhanced quantum sensing with non-Hermitian lattice dynamics. *Nat. Commun.* **11**, 5382 (2020).
29. Weidemann, S. et al. Topological funneling of light. *Science* **368**, 311 (2020).
30. Longhi, S. Non-hermitian gauged topological laser arrays. *Ann. der Phys.* **530**, 1800023 (2018).
31. Zhu, B. et al. Anomalous single-mode lasing induced by nonlinearity and the non-hermitian skin effect. *Phys. Rev. Lett.* **129**, 013903 (2022).
32. Kawabata, K., Shiozaki, K., Ueda, M. & Sato, M. Symmetry and topology in non-hermitian physics. *Phys. Rev. X* **9**, 041015 (2019).
33. Okuma, N., Kawabata, K., Shiozaki, K. & Sato, M. Topological origin of non-hermitian skin effects. *Phys. Rev. Lett.* **124**, 086801 (2020).
34. Gong, Z. et al. Topological phases of non-Hermitian systems. *Phys. Rev. X* **8**, 031079 (2018).
35. Denner, M. M. et al. Exceptional topological insulators. *Nat. Commun.* **12**, 5681 (2021).
36. Yi, Y. & Yang, Z. Non-Hermitian skin modes induced by on-site dissipations and chiral tunneling effect. *Phys. Rev. Lett.* **125**, 186802 (2020).
37. Borgnia, D. S., Kruchkov, A. J. & Slager, R.-J. Non-hermitian boundary modes and topology. *Phys. Rev. Lett.* **124**, 056802 (2020).
38. Li, X., Li, X. & Das Sarma, S. Mobility edges in one-dimensional bichromatic incommensurate potentials. *Phys. Rev. B* **96**, 085119 (2017).
39. Li, X. & Das Sarma, S. Mobility edge and intermediate phase in one-dimensional incommensurate lattice potentials. *Phys. Rev. B* **101**, 064203 (2020).
40. Yokomizo, K. & Murakami, S. Non-Bloch band theory and bulk Cedge correspondence in non-Hermitian systems. *Progress of Theoretical and Experimental Physics* **2020** (2020), <https://doi.org/10.1093/ptep/ptaa14012A102>, <https://academic.oup.com/ptep/article-pdf/2020/12/12A102/35611788/ptaa140.pdf>.
41. Delplace, P., Yoshida, T. & Hatsugai, Y. Symmetry-protected multifold exceptional points and their topological characterization. *Phys. Rev. Lett.* **127**, 186602 (2021).
42. Bergholtz, E. J., Budich, J. C. & Kunst, F. K. Exceptional topology of non-Hermitian systems. *Rev. Mod. Phys.* **93**, 015005 (2021).
43. Degen, C. L., Reinhard, F. & Cappellaro, P. Quantum sensing. *Rev. Mod. Phys.* **89**, 035002 (2017).
44. Alù, A. & Egheta, N. Cloaking a sensor. *Phys. Rev. Lett.* **102**, 233901 (2009).
45. Wang, C., Fu, Z., and Yang, L. Non-hermitian physics and engineering in silicon photonics, in *Silicon Photonics IV: Innovative Frontiers*, edited by Lockwood, D. J. and Pavesi, L. (Springer International Publishing, Cham, 2021) pp. 323–364.
46. Yin, K. et al. Wireless real-time capacitance readout based on perturbed nonlinear parity-time symmetry. *Appl. Phys. Lett.* **120**, 194101 (2022).
47. Tuniz, A., Schmidt, M. A. & Kuhlmeier, B. T. Influence of non-Hermitian mode topology on refractive index sensing with plasmonic waveguides. *Photon. Res.* **10**, 719 (2022).
48. Qin, G.-Q. et al. Experimental realization of sensitivity enhancement and suppression with exceptional surfaces. *Laser Photonics Rev.* **15**, 2000569 (2021).
49. Koch, F. & Budich, J. C. Quantum non-Hermitian topological sensors. *Phys. Rev. Res.* **4**, 013113 (2022).
50. Nikzamid, A. & Capolino, F. Highly sensitive coupled oscillator based on an exceptional point of degeneracy and nonlinearity. *Phys. Rev. Appl.* **18**, 054059 (2022).
51. Zhang, G.-Q. & You, J. Q. Higher-order exceptional point in a cavity magnonics system. *Phys. Rev. B* **99**, 054404 (2019).
52. Gou, W. et al. Tunable nonreciprocal quantum transport through a dissipative Aharonov-Bohm ring in ultracold atoms. *Phys. Rev. Lett.* **124**, 070402 (2020).
53. Xu, Y., Wang, S.-T. & Duan, L.-M. Weyl exceptional rings in a three-dimensional dissipative cold atomic gas. *Phys. Rev. Lett.* **118**, 045701 (2017).
54. Li, H., Cui, X. & Yi, W. Non-Hermitian skin effect in a spin-orbit-coupled Bose-Einstein condensate. *JUSTC* **52**, 2 (2022).
55. Zhou, L., Li, H., Yi, W. & Cui, X. Engineering non-Hermitian skin effect with band topology in ultracold gases. *Commun. Phys.* **5**, 252 (2022).
56. Zou, D. et al. Observation of hybrid higher-order skin-topological effect in non-Hermitian topoelectrical circuits. *Nat. Commun.* **12**, 7201 (2021).
57. Helbig, T. et al. Generalized bulk-boundary correspondence in non-Hermitian topoelectrical circuits. *Nat. Phys.* **16**, 747 (2020).
58. Lee, C. H. et al. Topoelectrical circuits. *Commun. Phys.* **1**, 39 (2018).
59. Yang, R. et al. Designing non-Hermitian real spectra through electrostatics. *Sci. Bull.* **67**, 1865 (2022).
60. Fleckenstein, C. et al. Non-Hermitian topology in monitored quantum circuits. *Phys. Rev. Res.* **4**, L032026 (2022).
61. Wu, J. et al. Non-Hermitian second-order topology induced by resistances in electric circuits. *Phys. Rev. B* **105**, 195127 (2022).
62. Hofmann, T., Helbig, T., Lee, C. H., Greiter, M. & Thomale, R. Chiral voltage propagation and calibration in a topoelectrical chern circuit. *Phys. Rev. Lett.* **122**, 247702 (2019).

63. Ezawa, M. Electric circuits for non-Hermitian Chern insulators. *Phys. Rev. B* **100**, 081401 (2019).
64. Cerjan, A. et al. Experimental realization of a Weyl exceptional ring. *Nat. Photonics* **13**, 623 (2019).
65. Chen, W., Kaya Özdemir, Ş., Zhao, G., Wiersig, J., and Yang, L., Exceptional points enhance sensing in an optical microcavity. *Nature* **13** <https://doi.org/10.1038/nature23281> (2017).
66. Ozawa, T. et al. Topological photonics. *Rev. Mod. Phys.* **91**, 015006 (2019).
67. Liu, J.-j et al. Experimental realization of weyl exceptional rings in a synthetic three-dimensional non-hermitian phononic crystal. *Phys. Rev. Lett.* **129**, 084301 (2022).
68. Fang, Z., Hu, M., Zhou, L. & Ding, K. Geometry-dependent skin effects in reciprocal photonic crystals. *Nanophotonics* **11**, 3447 (2022).

Acknowledgements

This work was supported by NSFC under Grant no. 11874190. National Key R&D Program of China under Grant Nos. 2021YFA1400900, 2021YFA0718300, 2021YFA1402100, NSFC under Grant no. 12174461, 12234012, 12334012, 52327808, Space Application System of China Manned Space Program. No. FRF-TP-22-098A1. 106-CK00042/132. We thank Chen Fang for useful discussions. We thank Liwen Bianji (Edanz) for editing the language of a draft of this manuscript.

Author contributions

G.-F.G. conceived the idea and performed the simulations. G.-F.G., X.-X.B., H.-J.Z. and X.-M.Z. wrote the paper. L.Z., L.T. and W.-M.L. supervised the work.

Competing interests

The authors declare no competing interests.

Additional information

Supplementary information The online version contains supplementary material available at <https://doi.org/10.1038/s42005-023-01487-4>.

Correspondence and requests for materials should be addressed to Lin Zhuang, Lei Tan or Wu-Ming Liu.

Peer review information *Communications Physics* thanks the anonymous reviewers for their contribution to the peer review of this work. A peer review file is available.

Reprints and permission information is available at <http://www.nature.com/reprints>

Publisher's note Springer Nature remains neutral with regard to jurisdictional claims in published maps and institutional affiliations.



Open Access This article is licensed under a Creative Commons Attribution 4.0 International License, which permits use, sharing, adaptation, distribution and reproduction in any medium or format, as long as you give appropriate credit to the original author(s) and the source, provide a link to the Creative Commons license, and indicate if changes were made. The images or other third party material in this article are included in the article's Creative Commons license, unless indicated otherwise in a credit line to the material. If material is not included in the article's Creative Commons license and your intended use is not permitted by statutory regulation or exceeds the permitted use, you will need to obtain permission directly from the copyright holder. To view a copy of this license, visit <http://creativecommons.org/licenses/by/4.0/>.

© The Author(s) 2023